# Nanoscale

Accepted Manuscript


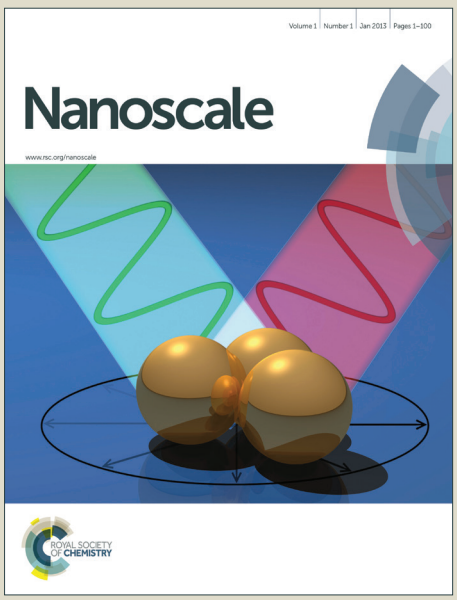





ROYAL SOCIETY OF CHEMISTRY

www.rsc.org/nanoscale

# Spin Seebeck effect and spin Hall magnetoresistance at high temperatures for Pt/yttrium iron garnet hybrid structure

Shuanhu Wang[1], Lvkuan Zou[1], Xu Zhang[1], Jianwang Cai[1], Shufang Wang[2ξ], Baogen Shen[1] and Jirong Sun[1]*

[1]Beijing National Laboratory for Condensed Matter Physics and Institute of Physics, Chinese Academy of Sciences, Beijing 100190, People's Republic of China

[2]College of Physics Science and Technology, Hebei University, Baoding 071002, Hebei Province, People's Republic of China

**Abstract**

Based on unique experimental setups, temperature dependences of longitudinal spin Seebeck effect (LSSE) and spin Hall magnetoresistance (SMR) of the Pt/ yttrium iron garnet (Pt/YIG) hybrid structure are determined in a wide temperature range up to the Curie temperature of YIG. From a theoretical analysis of the experimental relation between SMR and temperature, spin mixing conductance of the Pt/YIG interface is deduced as a function of temperature. Adopting the deduced spin mixing conductance, the temperature dependence of the LSSE is well reproduced based on the magnon spin current theory. Our researches shed new lights on the controversy about the theoretical models for the LSSE.

* jrsun@iphy.ac.cn

ξ swang2008@hotmail.com

## 1. Introduction

Due to the strong spin-orbit coupling of Pt and the distinct ferromagnetic properties of yttrium iron garnet (YIG), the spin and charge transport of the Pt/YIG hybrid structure exhibit abundant phenomena. An intriguing discovery is the spin Seebeck effect in Pt/YIG[1-5], stemming from thermal gradient-caused spin current injection from YIG into Pt. This effect provides a new approach for the generation and manipulation of spin current, thus has drawn great attentions in recent years. In addition to spin Seebeck effect, the spin Hall magnetoresistance (SMR) of Pt/YIG is also an interesting discovery[6]. It has been proven that the charge current in Pt produces a vertical spin current due to spin Hall effect, and the reflection of this spin current at the Pt/YIG interface then generates a charge current that is superimposed on the original one, leading to a new kind of magnetoresistance.

Although the physical image of the SMR is very clear, the mechanism for the spin Seebeck effect, particularly the longitudinal spin Seebeck effect (LSSE), is still in debate. Two representative theories have been presented by Xiao *et al.* and Rezende *et al.*, respectively. Xiao *et al.*[7-11] believed that the magnon, electron and phonon temperatures are different at the Pt/YIG interface, though the expected temperature differences are not observed from the analysis of the Brillouin light scattering spectroscopy,[12] and this generated a spin pumping into Pt, yielding the LSSE. Different from Xiao *et al.*, Rezende *et al.*[13] ascribed the LSSE to temperature gradient-generated magnon spin current across YIG, and presented a theory that well reproduced the temperature dependence of the LSSE obtained below room temperature. Both theories describe incoherent spin pumping, but, in the latter theory, magnon propagation & accumulation induced by heat current is taken into consideration. By studying the temporal evolution of LSSE, Agrawal *et al.*[14] found that the thermal gradient rose more faster than the LSSE signal, which means that the bulk magnon transport plays an important role in determining the LSSE. Despite the controversy of different theoretical models, there is a consensus that spin mixing conductance ($G$), spin Hall angle ($\theta_{sh}$), spin diffusion length ($\lambda_{Pt}$) are important factors affecting both the LSSE and the SMR. This implies that these two effects may mutually corroborate, leading to further insights into underlying physics.

We noted that most of the previous experiments on LSSE and SMR have been performed in the low temperature region, i.e., below room temperature. Data for high

temperature region, particularly near the Curie temperature ($T_C$) of YIG, are scarce because of experimental difficulties, though they are particularly important for elucidating the mechanisms of the LSSE and SMR. Recently, Uchida *et al.*[15] undertook the only study on high temperature LSSE, and observed a rapid decrease of the LSSE voltage ($V_{LSSE}$) with temperature, i.e., $V_{LSSE} \propto (T_C\text{-}T)^3$. It is a pity that the reported $V_{LSSE}$ fluctuates around zero in the temperature range from 450 and 520 K. This and the lacking of a simultaneous study on SMR make a comprehensive analysis of the LSSE and SMR difficult. Based on unique experimental setups, in this paper we determined the LSSE and the SMR for the same Pt/YIG hybrid structure in a wide temperature below $T_C$. From the SMR data, temperature-dependent spin mixing conductance was determined. A rapid decrease of $G$ with temperature is observed above 300 K, due to the reduction of the magnetization of YIG. Adopting the parameters deduced from the SMR, the temperature dependence of the LSSE is satisfactorily reproduced with the theory of magnon spin current. These analyses show that the spin mixing conductance of the Pt/YIG interface, the magnetization of YIG and the spin diffusion length of Pt strongly influence the LSSE.

## 2. Experiment

A 21-μm-thick single crystal YIG slab was first grown above (111)-oriented $Gd_3Ga_5O_{12}$ ($5\times3\times0.5$ mm$^3$) by liquid phase epitaxy, and then a Pt layer with a thickness of 7 nm or 30 nm was deposited, via magnetron sputtering, on the top of YIG through a Hall-bar-shaped mask. To generate a vertical thermal gradient ($\nabla$T), the sample was heated by a underneath ceramic heater that is pasted to the sample by silver epoxy. In this case, the temperature gradient is directed from bottom to top. An alternative method to generate thermal gradient is illuminating the top of the sample using laser beam while heating sample back with the heater[14, 16-18]. In this case, the thermal gradient is directed from top to bottom for the present laser power (30 mw). Magnetic field ($H$) is provided by a Helmholtz coil, applied along $x$-axis of the sample. Two electrodes aligning along $y$-axis are used to detect the LSSE voltage. The whole measurement unit, including the sample, the heater, the laser emitter and the Helmholtz coil, is sealed in an electromagnetic shielding box in ambient atmosphere. The SMR is measured using the physical property measurement system (PPMS) in the temperature range below 300 K and a home-made system above 300 K. Magnetic field is applied in the $x$-$y$ plane at an angle of 45$^o$ with respect to the $x$-axis. Laser is

30 mW in power and 660 nm in wavelength. The spot size of the laser is ~4.6 mm in diameter, nearly covering the whole Pt hall bar.

## 3. Results and discussions

Figures 1b and 1c show the magnetic field dependences of thermal voltage, recorded in the temperature range from 300 K to 516 K in the thermal gradient generated by heater alone (1b) and heater plus laser (1c), respectively. Around ambient temperature, as shown in figure 1b, the sample is at thermal equilibrium with environment and no thermoelectric voltage changes are observed for magnetic cycling. $V_{LSSE}$ appears when the sample is heated above 300 K, grows with heating power and, after a maximum value of 1 μV at ~445 K, decreases rapidly. This complex behavior could be jointly determined by the variation of thermal gradient, magnetization and thermal conductivity of YIG[7]. Under the combined influence of heater and laser beam, an opposite $V_{LSSE}$-$H$ loop is detected up to 489 K, implying a reversion of thermal gradient direction. Possibly, laser heating generates a local thermal gradient that over-counteracts that of the heater. In this case, the $V_{LSSE}$ is maximal at room temperature, and continuously decreases with the increase of temperature. Figure 1d is a summary of the LSSE voltage, deduced from the difference of the two thermoelectric voltages under, respectively, a positive and a negative saturation field. It clearly shows the systematic variation of $V_{LSSE}$ with temperature.

Obviously, the complex temperature dependence of $V_{LSSE}$ in figure 1d is determined by the variations of thermal gradient, magnetization of YIG, spin mixing conductance of Pt/YIG, spin diffusion length of Pt, and *etc*. To get a quantitative description of the LSSE, it is necessary to determine the thermal gradient as a function of temperature. In general, a direct measurement of the temperature difference for the top and bottom planes of YIG will cause considerable experimental errors. As an alternative, we adopted a two-dimensional finite element model (2D FEM) to simulate the temperature distribution in YIG. During the simulation, the bottom plane of YIG was set to a temperature between 300 K and 560 K, and the environment to 300 K. Heat exchange was assumed to occur on top surface, via thermal radiation. Parameters involved in this simulation such as heat conductivity and heat capacity are obtained from Refs.[19] and [20]. Please refer to Appendix A for details of the FEM calculation. As an example, the thermal distributions for an average sample temperature of 415 K are shown in figures. 2c and 2d, respectively

corresponding to the cases with and without laser illumination. Since the Pt strip for thermoelectric measurements locates exactly at the middle of the top plane of YIG, we choose the temperature distribution just underneath the Pt strip to evaluate thermal gradient (dashed line in figures. 2c and 2d). Since temperature changes linearly from the top to the bottom of YIG, the thermal gradient is a constant. Figure 2e shows the deduced ∇T as a function of sample temperature. As expected, the thermal gradient generated by heater exhibits a monotonic growth with sample temperature, varying from 0 to 540 K/m as temperature increases from 300 K to 530 K. In contrast, the ∇T produced by combined heater and laser shows a direction reversion at ~475 K. Below ~475 K, the effect of local heating by laser is dominant, and ∇T points to the *-z* direction. However, with the increase of temperature, the effect of the heater finally counteracts that of laser, and the direction of ∇T is reversed. We noted that, at room temperature, the ∇T generated here by laser is similar to that obtained by Agrawal *et al*.[14] using a laser of 70 mW.

Based on the results of the 2D FEM calculations, we get the temperature dependence of $V_{LSSE}/\nabla T$ in figure 3a. The $V_{LSSE}/\nabla T$ data for two different heating methods coincide with each other satisfactorily. The meaning of this result is two-fold. First, the temperature gradient thus obtained is reasonable. Second, the experiment data are reliable. As shown in figure 3a, $V_{LSSE}/\nabla T$ is ~10 nVm/K at 300 K, decreases monotonically with the increase of temperature, and vanishes as $T$ approaches $T_C$. We also performed the experiments for a sample with a thicker Pt strip (30 nm), and observed a similar temperature dependence (inset in figure 3a). These results reveal a weakening of the LSSE as temperature approaches $T_C$, qualitatively agreeing with those of Uchida *et al.*[15]

Plotting $V_{LSSE}/\nabla T$ against $T_C$-$T$ in double logarithmic scale, we obtained a well linear relation that shows a slope of ~1.5. This means a critical exponent lower than that reported by Uchida *et al*.[15] The YIG film employed here is much thinner than that used by Uchida *et al*. (21 μm vs. 1 mm). This could by a reason for this difference noting the variation of the temperature dependence of the LSSE with the YIG thickness.[21] A similar analysis was performed on the data of 30 nm Pt, and the same temperature dependence of $V_{LSSE}$ was observed, which reveals the generality of these phenomena.

Obviously, the magnetization of YIG, the spin Hall angle of Pt and the spin

mixing conductance of the Pt/YIG interface may vary significantly with temperature, especially as $T$ approaches $T_C$. All these will affect the LSSE, resulting in a dramatic variation of the $V_{LSSE}$ with $T$. To understand the specific temperature dependence, a thorough analysis of the $V_{SSE}$-$T$ relation is desired. As afore stated, there is a consensus that spin mixing conductance, spin Hall angle, spin diffusion length are important factors determining both the LSSE and the SMR. Considering the fact different effects may mutually corroborate with each other, an investigation on the temperature dependence of the SMR may be helpful for a thorough understanding of the $V_{SSE}$-$T$ dependence. Figure 4a is schematic showing of the experimental setup. A relative large measuring current of 500 μA was applied along the Pt layer in order to offset the unbalanced LSSE voltage background generated by thermal irradiation. This current will not generate significant Joule heating as demonstrated by previous researches[22]. The voltage signals were collected from two transversally aligned electrodes, as a function of magnetic field which is applied at an angle of 45° with respect the $x$-axis (also the easy magnetization axis of YIG) and cycled between -100 Oe and 100 Oe. Here transversal resistivity $\rho_{xy}$ is acquired to characterize the SMR because of its low background signal thus high signal-to-noise ratio. Figure 4b shows $\rho_{xy}$ as a function of applied field, measured at different temperatures. $\rho_{xy}$ is nearly constant above saturation field, increases rapidly as $H$ decreases and gets a maximum at $H$=0. These are typical features of the SMR. With the decrease of temperature, the resistivity change $\Delta\rho_{xy}$ exhibits first a rapid growth, when temperature is high, and then a slow decrease, when temperature is low, leaving a local maximum of $5.6\times10^{-4}$ at ~97.6 K (figure 4c).

In general, from the temperature dependence of the SMR, additional information can be obtained, on such as spin mixing conductance, spin Hall angle, and spin diffusion length. As reported, the SMR can be well described by

$$\frac{\Delta\rho_{xy}}{\rho} = \theta_{sh}^2 \frac{\lambda_{Pt}}{t_{Pt}} \frac{2\lambda_{Pt} G tanh^2 \frac{t_{Pt}}{2\lambda_{Pt}}}{\sigma_{Pt} + 2\lambda_{Pt} G coth \frac{t_{Pt}}{\lambda_{Pt}}}, \quad (1)$$

where $\theta_{sh}$, $\lambda_{Pt}$, $t_{Pt}$ and $\sigma_{Pt}$ are spin Hall angle, spin diffusion length, thickness and conductivity of Pt, respectively. The equality $\Delta\rho_{xy}=\Delta\rho_{xx}$ has been adopted here[6, 23].

Through a careful analysis, Marmion *et al.*[24] found that temperature dependence of SMR is mainly affected by $\lambda_{Pt}$ below room temperature,[25] determined by the

Elliot-Yafet mechanism for spin relaxation. Alternatively, Meyer *et al.*[26] ascribed the variation of SMR to a decrease in $\theta_{sh}$ instead of $\lambda_{Pt}$. According to Meyer *et al.*, $\theta_{sh}$ changes obviously below 100 K whereas remains nearly constant above 100 K. In contrast, Isasa *et al.*[27] declared that $\theta_{sh}$ was relatively weakly temperature-dependent, and the $\lambda_{Pt}$ decay with temperature, in the form of Elliot-Yafet, is the origin of the temperature effects. Obstbaum *et al.*[28] studied the inverse spin Hall effect and anisotropic magnetoresistance for the Pt/permalloy structure, and found that a good agreement of experimental results with theoretical ones is gained only when $\theta_{sh}$ is a constant. As for $G$, both Marmion[24] and Meyer[26] treated it as a constant below 300 K, independent of temperature.

Basing on the above works, we firstly fit our experimental data to Eq. (1), adopting a constant $\theta_{sh}$ (0.085), $G$ ($9\times10^{14}$ $\Omega^{-1}m^{-2}$), and a varied $\lambda_{Pt}$ of the Elliot-Yafet form ($\lambda_{Pt}=3\times10^{-7}/T$ in unit of nm). As shown by figure 4c, although the experimental data (symbols) can be satisfactorily reproduced at low temperatures (black curve), obvious deviations appear above 280 K. Considering the obvious change of the magnetic properties of YIG with temperature, high temperature may mainly influence spin mixing conductance. Therefore, setting $G$ to a constant could be inadequate at high temperatures. By setting $G$ to

$$G = \frac{\sigma_{Pt}}{\left( \frac{2\lambda_{Pt}\theta_{sh}^2 G\lambda_{Pt} tanh^2\left(\frac{t_{Pt}}{2\lambda_{Pt}}\right)}{\frac{\Delta\rho_{xy}}{\rho}\cdot t_{Pt}} - 2\lambda_{Pt} coth\left(\frac{t_{Pt}}{\lambda_{Pt}}\right) \right)}, \qquad (2)$$

we obtained the temperature dependence $G$ shown in figure 5. $G$ is nearly constant below 280 K and decreases linearly with temperature above 280 K, where $\theta_{sh}$ has been set to 0.085, and $\sigma_{Pt}$ has been obtained by direct measurements. Indeed, reduced magnetization of YIG causes a reduction in $G$. We noted that a similar $G$-$T$ relations has been theoretical prediction by Ohnuma *et al.*[29] and experimentally deduced by Uchida *et al.*[30] The red curve in figure 4c demonstrates the self-consistent fitting of the SMR data.

Adopting the deduced $G$-$T$ relation, the temperature dependence of $V_{LSSE}$ can be calculated based on different theoretical models. Xiao *et al.* proposed a model based on the spin pumping generated by the difference of magnon and electron (phonon) temperatures [Eq. (B1) in Appendix B][7-10]. Later, Rezende *et al.*[9] presented an

alternative model based on the bulk magnon spin current in YIG, generated by thermal gradient (Eq. (B5) in Appendix B). In the latter model, the temperature dependence of magnon lifetime is considered, and a rigid magnon dispersion relation is adopted. Eq. (B5) has well explained the temperature dependence of the LSSE below room temperature. Details of these two theories are presented in Appendix B. Parameters involved in Eqs. (B1) and (B5) can be directly measured, such as the resistivity of Pt, or indexed from references (refer to Appendix B for details).

In figure 6 we show a comparison of the experimental (symbols) and theoretical (solid curves) results. The olive and blue curves are calculated by the theories of Xiao *et al*. and Rezende *et al.*, respectively. Different from the experimental result, the theoretical $V_{LSSE}/\nabla T$ of Xiao *et al*. displays a progressive increase with temperature to a local maximum at ~470 K, before a drastic drop at higher temperatures. It is not clear at present whether the oversimplified magnon dispersion relation of this theory is responsible for this strong deviation. In contrast, the magnon spin current theory proposed by Rezende *et al*. yields results that are in good agreement with the experimental ones. The slight deviations in the temperature interval from 400 K to 500 K could be ascribed to inaccurate parameters adopted for the calculations (for example, the magnon diffusion length $l_m$ may be temperature dependent rather than independent[31]). It implies that the LSSE can be produced without referring to the difference of magnon and phonon temperatures at the Pt/YIG interface. According to this theory, the LSSE is associated with magnon spin current across YIG, and it is thus a bulk effect. Recently, Etesami *et al.*[32] presented a model by solving the stochastic Landau-Lifshitz-Gilbert equation, and they found that the LSSE can be an effect of magnon accumulation, quantified by exchange spin torque, which also support the scenario of bulk origin of the LSSE.

## 4. Summary

Temperature dependence of the LSSE and SMR has been experimentally studied for the Pt/YIG hybrid structure. Based on two different experimental setups, two sets of LSSE voltages that coincide with each other have been obtained as functions of sample temperature, adopting the thermal gradients determined by finite element calculations. Simultaneously, SMR was recorded as a function temperature. Though the analysis of SMR, spin mixing conductance is derived. The decrease of magnetization of YIG results in a linear reduction of spin mixing conductance with

temperature when the latter is higher 300 K. Adopting the deduced spin mixing conductance and independently adjusted spin diffusion length and spin Hall angle, the temperature dependence of the LSSE is well reproduced based on the magnon spin current theory. The present work provides a deep insight to the mechanism of the LSSE and other spin transport process in the Pt/YIG hybrid structure.

**Acknowledgement**

This work has been supported by the National Basic Research of China (Grant Nos. 2011CB921801, 2012CB921403, and 2013CB921701), the National Natural Science Foundation of China (Grant Nos. 11074285, 51372064, and 11134007), and the Strategic Priority Research Program of the Chinese Academy of Sciences (XDB07030200).

## Appendix A: Detail in 2D FEM

For the temperature gradient induced by thermal radiation,

$$k\nabla T = \varepsilon\sigma(T_{amb}^4 - T^4) \quad \text{(A1)}$$

where $k$ is thermal conductivity of YIG and $T_{amb}$ is the ambient temperature which is 300 K. For YIG, $\varepsilon_{YIG}$=0.5.[33] $k$ is calculated by $k=DC_p\rho$, where $D$, $C_p$ and $\rho$ are thermal diffusivity, heat capacity and density. For YIG, $\rho$=5170 kg/m$^3$,[34] and temperature dependences of $D$ and $c_p$ are extracted for Refs.[19, 20], respectively.

The reflectivity at the interface between layer i-1 and layer i is calculated by Fresnel equation [9]

$$R = \left|\frac{n_{i-1} - n_i}{n_{i-1} + n_i}\right|^2, \quad \text{(A2)}$$

where $n_i$ denotes the refractive index[35-37]. And we get $R_{Pt/air}$= 0.17, $R_{YIG/Pt}$= 0.009, $R_{YIG/air}$=0.15. There are two kinds of surface exposed to the illumination. The one is covered by Pt and the other is not as shown in figure A1.

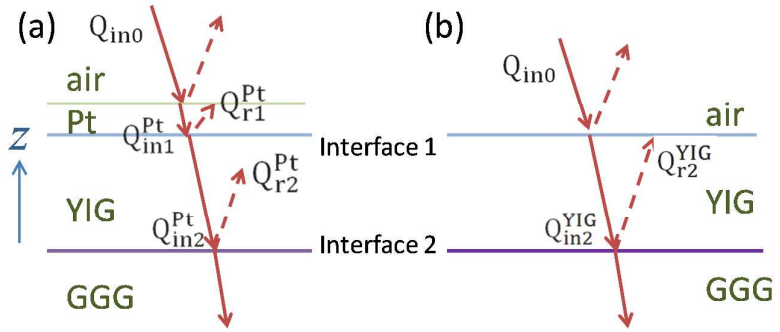


**Figure A1.** Sample surface coved by Pt (a) and YIG (b).

For surface covered by Pt, reflected energy as shown in figure A1 $Q_{r1}^{Pt} \approx 0$, $Q_{r2}^{Pt} \approx 0$. The energy of laser is $Q_{in0}$=2.5mW/mm$^2$. Input energy at the interface between Pt and YIG (noted as 1) after reflected and absorbed by Pt is

$$Q_{in1}^{Pt}\,(z_{Pt} = 7\,nm) = Q_{in0}\left(1 - R_{Pt/air}\right)e^{-\alpha_{Pt}z_{Pt}} = 0.468\ Q_{in0}. \quad (A3)$$

Energy passed through YIG film is

$$Q_{in2}^{Pt}\,(z_{YIG} = 20\,\mu m) = Q_{in1}^{Pt}\left(1 - R_{YIG/Pt}\right)e^{-\alpha_{YIG}z_{YIG}} = 0.172\ Q_{in0}. \quad (A4)$$

So the energy absorbed by YIG in this case is

$$Q_{abs}^{Pt} = Q_{in1}^{Pt} - Q_{in2}^{Pt} - Q_{r2} = 0.296\ Q_{in0}. \quad (A5)$$

For surface covered by YIG, energy passed through YIG film is

$$Q_{in2}^{YIG}\,(z_{YIG} = 20\,\mu m) = Q_{in0}\left(1 - R_{YIG/air}\right)e^{-\alpha_{YIG}z_{YIG}} = 0.313\ Q_{in0}. \quad (A6)$$

Here energy absorbed by YIG is

$$Q_{abs}^{YIG} = Q_{in0} - Q_{in2}^{YIG} - Q_{r2}^{YIG} = 0.537\ Q_{in0}. \quad (A7)$$

Due to the fact that the ratio of surface covered by Pt and YIG is 15:85, the total energy absorbed by YIG is

$$Q_{abs} = 0.15\,Q_{abs}^{Pt} + 0.85 Q_{abs}^{YIG} = 1.25\ mW/mm^2. \quad (A8)$$

So during the FEM calculation, we apple a heat flow with density of 1.25 mW/mm$^2$ to the YIG film.

**Appendix B: Two kinds of theories for LSSE**

Based on the interfacial thermal spin pumping mechanism[7, 8, 10] and the quadratic dispersion relation, Xiao *et al.*[7, 8] and Weiler *et al*[10]. find the inverse spin Hall effect voltage detected by Pt of

$$V_{LSSE} = \frac{g\gamma\hbar k_B}{2\pi M_s V_a}\theta_{sh}\rho_{Pt}l_{Pt}\cdot\Delta T, \quad (B1)$$

where the $V_a$ is magnetic coherence volume and it is given by

$$V_a = \frac{2}{3\zeta(5/2)}\left(\frac{4\pi S}{k_B T}\right)^{3/2}. \quad (B2)$$

$\hbar$ and $k_B$ are reduced Plank and Boltzmann constant. $g$ is the spin mixing conductance per unit of interface area and the conductance quantum: $g$=$Gh/e^2$. $M_s$ , $\gamma$ and $S$ are the saturation magnetization, gyromagnetic ratio and spin wave stiffness of YIG, respectively. It is reported that spin wave stiffness is proportional to magnetization[38, 39], so

$$\frac{S(T)}{M(T)} = \frac{S(0)}{M(0)}. \quad \text{(B3)}$$

At room temperature, $S(300\ K)=8.5*10^{-40}$ $Jm^2$ (Ref. 39). $\theta_{sh}$ is the spin-Hall angle of Pt which is shown to exhibit weak temperature dependence especially above 100 $K$.[27, 28]

The mechanism proposed by Rezende *et al.*[13] for LSSE is based on the magnon spin current generated in the bulk of the Pt, which provide continuity for the spin flow. The magnon dispersion relation is

$$\omega_k = \omega_{ZB}\left(1 - cos\frac{\pi k}{2k_m}\right), \quad \text{(B4)}$$

where $\omega_{ZB}$ is the zone boundary frequency and $k_m$ is the value of the maximum wave number[13]. They also considered magnon lifetime as a strong function of the wave number and found the spin current injected into Pt is

$$J_S^z = -\frac{\gamma\hbar\rho k_m^3 l_m}{4\pi M\pi^2}\frac{B_1 B_s}{B_2} g k_B \nabla T, \quad \text{(B5)}$$

where $\rho$ is the effect of the finite FMI layer thickness, noted as

$$\rho = \frac{cosh(t_{FM}/l_m) - 1}{sinh(t_{FM}/l_m)}. \quad \text{(B6)}$$

$k_m$ is the value of the maximum wave number:

$$\mathrm{k_m} = \sqrt{3} \times 2.5/a_l = 2 \times 10^{-7}\mathrm{cm}^{-1},$$

$a_l$ being the lattice parameter, and magnon diffusion length $l_m$=70 nm. The integrals $B_1$, $B_2$ and $B_3$ is noted as

$$B_1 = \int_0^1 q^2 \frac{xe^x}{(e^x-1)^2} dq, \quad (B7a)$$

$$B_2 = \int_0^1 q^2 sin^2\left(\frac{\pi q}{2}\right)\frac{e^x}{\eta_q(e^x-1)^2} dq \text{ and} \quad (B7b)$$

$$B_s = \int_0^1 q^2 sin^2\left(\frac{\pi q}{2}\right)\frac{e^x x}{\eta_q(e^x-1)^2} dq, \quad \text{(B7c)}$$

where $x=\hbar\omega_k/(k_B/T)$, $q=k_m/k$, and $\eta_q$=1+500$q$($T$/300)+(5100$q^2$-3250$q^3$)($T$/300)$^2$. By integrating the charge-current density along Pt layer, the inverse spin Hall effect voltage detected in Pt becomes[40]

$$V_{LSSE} = R_{Pt}\omega\lambda_{Pt}\frac{2e}{\hbar}\theta_{SH}\, tanh\left(\frac{t_{Pt}}{2\lambda_{Pt}}\right)\cdot J_S^z \quad \text{(B8)}$$

where $R_{Pt}$, $\omega$ and $t_{Pt}$ are resistance, thickness and width of Pt strip, respectively.

## References


1. K. Uchida, H. Adachi, T. Ota, H. Nakayama, S. Maekawa and E. Saitoh, *Appl Phys Lett*, 2010, **97**, 172505-172503.
2. T. Kikkawa, K. Uchida, Y. Shiomi, Z. Qiu, D. Hou, D. Tian, H. Nakayama, X. F. Jin and E. Saitoh, *Phys Rev Lett*, 2013, **110**, 067207.
3. J. H. Han, C. Song, F. Li, Y. Y. Wang, G. Y. Wang, Q. H. Yang and F. Pan, *Physical Review B*, 2014, **90**, 144431.
4. T. Liao, J. Lin, G. Su, B. Lin and J. Chen, *Nanoscale*, 2015, **7**, 7920-7926.
5. D. Matatagui, O. V. Kolokoltsev, N. Qureshi, E. V. Mejia-Uriarte and J. M. Saniger, *Nanoscale*, 2015, **7**, 9607-9613.
6. H. Nakayama, M. Althammer, Y. T. Chen, K. Uchida, Y. Kajiwara, D. Kikuchi, T. Ohtani, S. Geprags, M. Opel, S. Takahashi, R. Gross, G. E. Bauer, S. T. Goennenwein and E. Saitoh, *Phys Rev Lett*, 2013, **110**, 206601.
7. J. Xiao, G. E. W. Bauer, K.-c. Uchida, E. Saitoh and S. Maekawa, *Physical Review B*, 2010, **81**, 214418.
8. J. Xiao, G. E. W. Bauer, K.-c. Uchida, E. Saitoh and S. Maekawa, *Physical Review B*, 2010, **82**, 099904.
9. M. Schreier, A. Kamra, M. Weiler, J. Xiao, G. E. W. Bauer, R. Gross and S. T. B. Goennenwein, *Physical Review B*, 2013, **88**, 094410.
10. M. Weiler, M. Althammer, M. Schreier, J. Lotze, M. Pernpeintner, S. Meyer, H. Huebl, R. Gross, A. Kamra, J. Xiao, Y. T. Chen, H. Jiao, G. E. Bauer and S. T. Goennenwein, *Phys Rev Lett*, 2013, **111**, 176601.
11. J. C. Rojas-Sanchez, N. Reyren, P. Laczkowski, W. Savero, J. P. Attane, C. Deranlot, M. Jamet, J. M. George, L. Vila and H. Jaffres, *Physical Review Letters*, 2014, **112**, 106602.
12. M. Agrawal, V. I. Vasyuchka, A. A. Serga, A. D. Karenowska, G. A. Melkov and B. Hillebrands, *Physical Review Letters*, 2013, **111**, 107204.
13. S. M. Rezende, R. L. Rodriguez-Suarez, R. O. Cunha, A. R. Rodrigues, F. L. A. Machado, G. A. F. Guerra, J. C. L. Ortiz and A. Azevedo, *Physical Review B*, 2014, **89**, 014416.
14. M. Agrawal, V. I. Vasyuchka, A. A. Serga, A. Kirihara, P. Pirro, T. Langner, M. B. Jungfleisch, A. V. Chumak, E. T. Papaioannou and B. Hillebrands, *Physical Review B*, 2014, **89**, 224414.
15. K. Uchida, T. Kikkawa, A. Miura, J. Shiomi and E. Saitoh, *Physical Review X*, 2014, **4**, 041023.
16. M. Walter, J. Walowski, V. Zbarsky, M. Munzenberg, M. Schafers, D. Ebke, G. Reiss, A. Thomas, P. Peretzki, M. Seibt, J. S. Moodera, M. Czerner, M. Bachmann and C. Heiliger, *Nat Mater*, 2011, **10**, 742-746.
17. M. Weiler, M. Althammer, F. D. Czeschka, H. Huebl, M. S. Wagner, M. Opel, I. M. Imort, G. Reiss, A. Thomas, R. Gross and S. T. Goennenwein, *Phys Rev Lett*, 2012, **108**, 106602.
18. W. Lin, M. Hehn, L. Chaput, B. Negulescu, S. Andrieu, F. Montaigne and S. Mangin, *Nat Commun*, 2012, **3**, 744.
19. M. Guillot, F. Tchéou, A. Marchand, P. Feldmann and R. Lagnier, *Z. Physik B - Condensed Matter*, 1981, **44**, 53-57.
20. A. M. Hofmeister, *Physics and Chemistry of Minerals*, 2006, **33**, 45-62.
21. **T. Kikkawa, K. Uchida, S. Daimon, Z. Y. Qiu, Y. Shiomi, and E. Saitoh**, *Physical Review B***,** 2015, **92,** 064413
22. W. X. Wang, S. H. Wang, L. K. Zou, J. W. Cai, Z. G. Sun and J. R. Sun, *Appl Phys Lett*, 2014, **105**,

182403.

23. Y.-T. Chen, S. Takahashi, H. Nakayama, M. Althammer, S. Goennenwein, E. Saitoh and G. Bauer, *Physical Review B*, 2013, **87**, 144411.
24. S. R. Marmion, M. Ali, M. McLaren, D. A. Williams and B. J. Hickey, *Physical Review B*, 2014, **89**, 220404.
25. R. J. Elliott, *Phys Rev*, 1954, **96**, 266-279.
26. S. Meyer, M. Althammer, S. Geprags, M. Opel, R. Gross and S. T. B. Goennenwein, *Appl Phys Lett*, 2014, **104**, 242411.
27. M. Isasa, E. Villamor, L. E. Hueso, M. Gradhand and F. Casanova, *Physical Review B*, 2015, **91**, 024402.
28. M. Obstbaum, M. Härtinger, H. G. Bauer, T. Meier, F. Swientek, C. H. Back and G. Woltersdorf, *Physical Review B*, 2014, **89**.
29. Y. Ohnuma, H. Adachi, E. Saitoh and S. Maekawa, *Physical Review B*, 2014, **89**, 174417.
30. K. Uchida, Z. Y. Qiu, T. Kikkawa, R. Iguchi and E. Saitoh, *Appl Phys Lett*, 2015, **106**, 052405.
31. S. R. Boona and J. P. Heremans, *Physical Review B*, 2014, **90**, 064421.
32. S. R. Etesami, L.Chotorlishvili, A. Sukhov, and J. Berakdar, *Physical Review B*, 2014, **90**, 014410
33. A. E. White, *Experimental study of electron temperature fluctuations in the DIII-D tokamak*, ProQuest, 2008.
34. A. E. Clark and R. E. Strakna, *Journal of Applied Physics*, 1961, **32**, 1172-&.
35. in *Handbook of Optical Constants of Solids*, ed. E. D. Palik, Academic Press, Burlington, 1997, DOI: http://dx.doi.org/10.1016/B978-012544415-6.50000-5, pp. xv-xvi.
36. G. B. Scott, D. E. Lacklison and J. L. Page, *Physical Review B*, 1974, **10**, 971-986.
37. P. Potera, S. Ubizskii, D. Sugak and K. Schwartz, *Acta Phys Pol A*, 2010, **117**, 181-183.
38. S. Bhagat, H. Lessoff, C. Vittoria and C. Guenzer, *physica status solidi (a)*, 1973, **20**, 731-738.
39. C. M. Srivastava and R. Aiyar, *J Phys C Solid State*, 1987, **20**, 1119-1128.
40. A. Azevedo, L. H. Vilela-Leao, R. L. Rodriguez-Suarez, A. F. L. Santos and S. M. Rezende, *Physical Review B*, 2011, **83**, 144402.

**Figure captions:**

**Fig. 1** (a) A schematic showing of the experimental setup for the LSSE study. A ceramic heater is placed underneath Pt/YIG and a laser beam is focused on sample surface. The average temperature of the sample is measured by a Pt100 thermometer on heater. (b) and (c) Magnetic field dependences of the thermal voltage across the Pt bar, generated by the thermal gradient of heater (b) and heater plus laser (c), respectively. (d) LSSE voltage as a function of temperature.

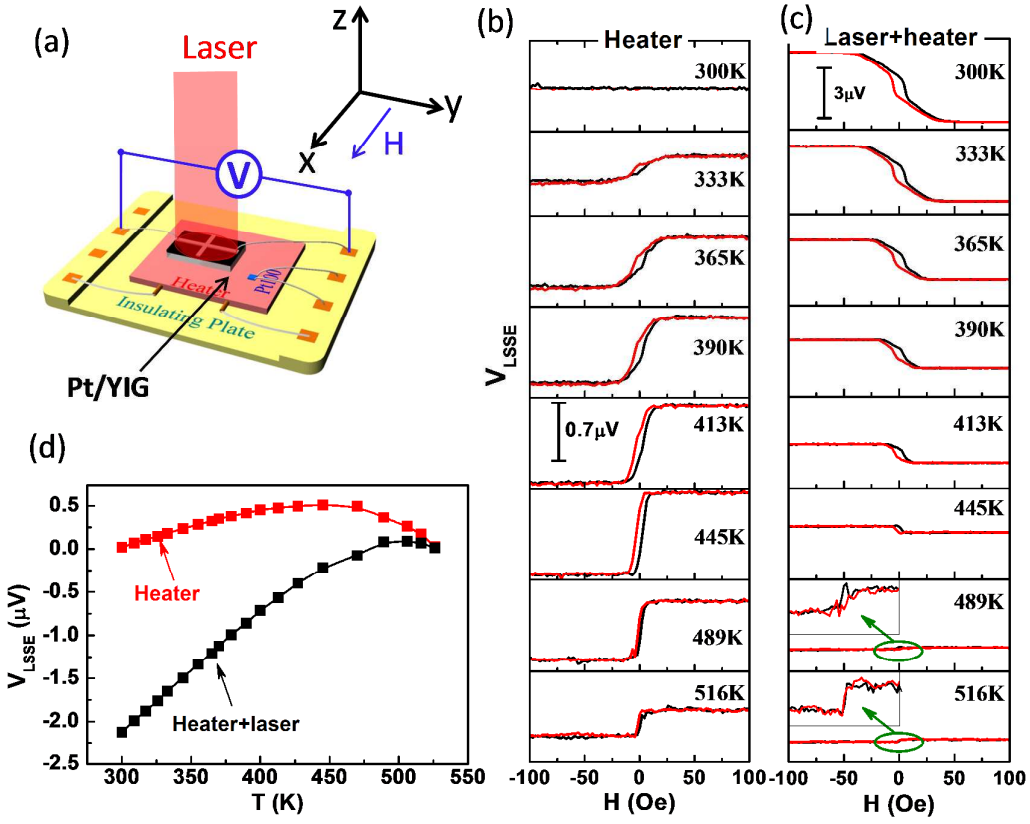

**Fig. 2** Experiment setups for the generation of thermal gradient by heater (a) and heater plus laser (b). (c) and (d) Temperature distribution in YIG on the cross section just below the Pt strip for thermoelectric measurements. The average sample temperature is 413 K. (e) Temperature gradient as a function of sample temperature, obtained along the middle of the YIG (marked by dashed lines).

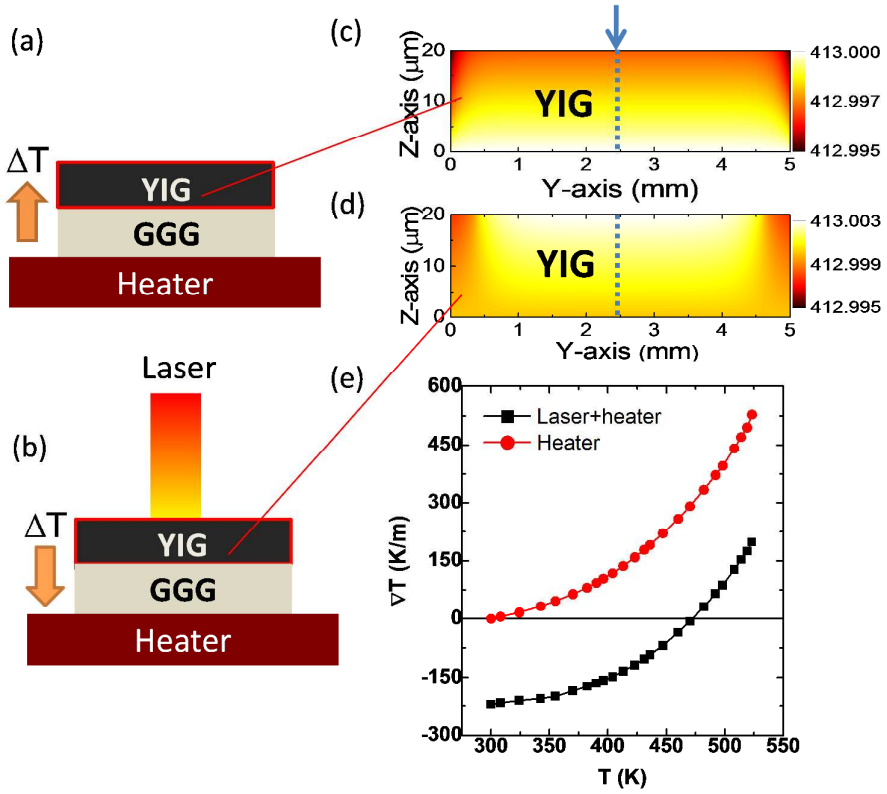

**Fig. 3** (a) Temperature dependence of $V_{LSSE}/\nabla T$ for two different heating methods. Inset shows the data of the sample with a thicker Pt strip (30 nm). (b) Double logarithmic plot of the $T_C$-$T$ dependence of $V_{LSSE}/\nabla T$. Solid line is a guide for the eye.

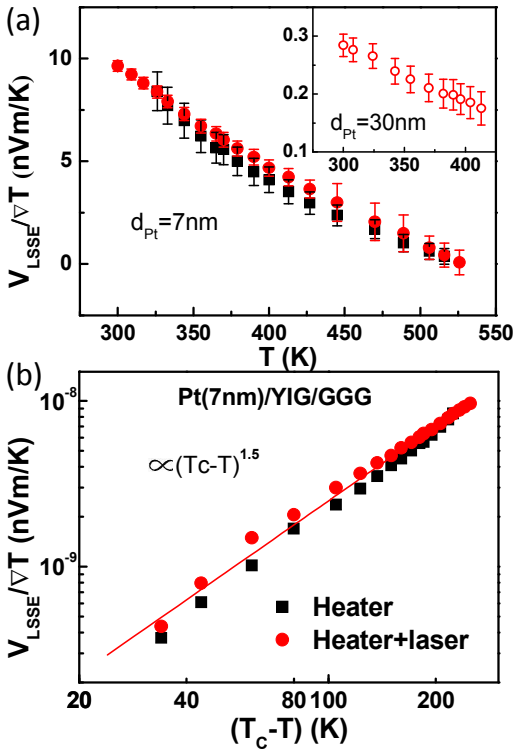

**Fig. 4** Experimental setup for the measurement of SMR. A heater is used to heat the sample. (b) Magnetic field dependence of the transversal resistivity $\rho_{xy}$ above 300 K. (c) Comparison of the experimental SMR (empty symbols) with theoretical results (solid lines). The black and red curves are calculated by Eq. (1) adopting a constant and a varied spin mixing conductance (G), respectively.

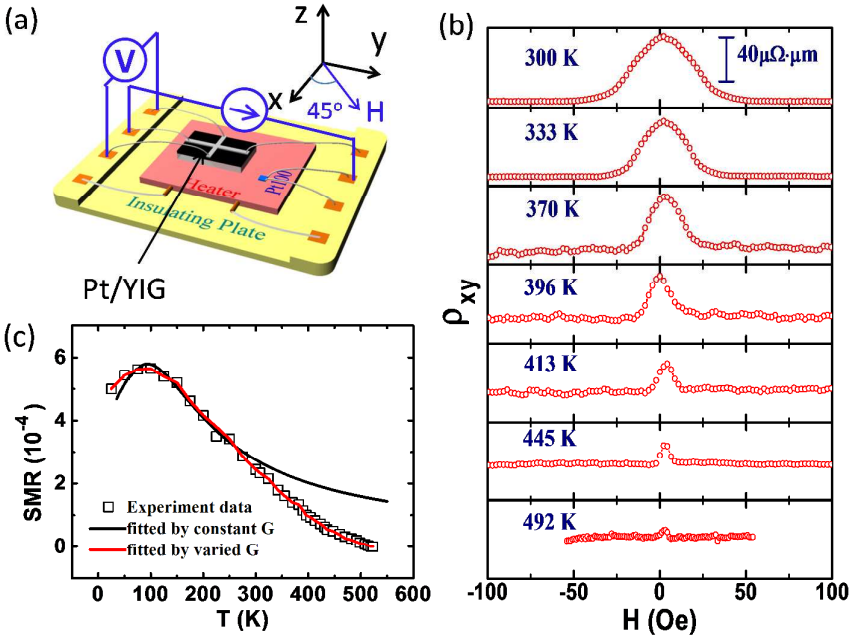

**Fig. 5** Temperature dependence of spin mixing conductance $G$ deduced from SMR based on Eq. (2).

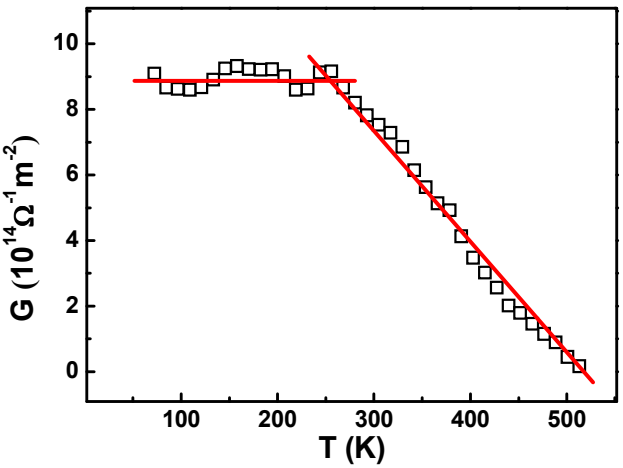

**Fig. 6** Comparison of experimental (symbols) and theoretical (solid curves) results. Olive and blue curves are obtained from the theories proposed by Xiao *et al.* and Rezende *et al.*, respectively.